Journal of Alloys and Compounds 520 (2012) 77–82

Contents lists available at SciVerse ScienceDirect

Journal of Alloys and Compounds

journal homepage: www.elsevier.com/locate/jallcom

Electrostatic spray deposition of porous $Fe_2V_4O_{13}$ films as electrodes for Li-ion batteries

Si-Rong Li [a], Nulati Yesibolati [a], Yu Qiao [a], Si-Yuan Ge [a], Xu-Yong Feng [a], Jun-Fa Zhu [b], Chun-Hua Chen [a,*]

[a] CAS Key Laboratory of Materials for Energy Conversion, Department of Materials Science and Engineering, University of Science and Technology of China, Anhui Hefei 230026, China
[b] National Synchrotron Radiation Laboratory, Anhui Hefei 230026, China

ARTICLE INFO

Article history:
Received 23 September 2011
Received in revised form
19 December 2011
Accepted 19 December 2011
Available online 21 January 2012

Keywords:
Electrostatic spray deposition
Thin film
Iron vanadate
Lithium ion battery
Electrode material

ABSTRACT

Porous thin films composed of complex Fe/V oxides (crystalline $Fe_2V_4O_{13}$ and amorphous $Fe_2V_4O_{12.29}$) are prepared by electrostatic spray deposition technique. The crystalline $Fe_2V_4O_{13}$ thin film shows a high initial capacity of 409 mAh g^{-1}. The cyclic voltammetry analysis of a $Fe_2V_4O_{13}$/Li cell reveals that the crystalline $Fe_2V_4O_{13}$ undergoes an irreversible phase transition when the lower cut-off voltage is below 2.5 V. Compared with the crystalline $Fe_2V_4O_{13}$, the amorphous $Fe_2V_4O_{12.29}$ thin film delivers a lower initial capacity of 349.9 mAh g^{-1} but exhibits better cycling performance in the voltage range of 1.0–4.0 V. After 50 cycles, its capacity can still reach around 200 mAh g^{-1}. X-ray photoelectron spectroscopy (XPS) reveals that the $Fe_2V_4O_{12.29}$ thin film contains ions of mixed valence states V^{5+}/V^{4+} and Fe^{3+}/Fe^{2+}, resulting in better rate capability for $Fe_2V_4O_{12.29}$ than for $Fe_2V_4O_{13}$. These results indicate that the amorphous Fe/V-oxide film is a promising electrode material for high energy applications.

1. Introduction

Rechargeable lithium-ion batteries (LIBs) hold a great potential for applications in electric vehicles (EVs) and hybrid electric vehicles (HEVs) owing to their high energy density, long lifespan and environment friendliness. Among various cathode materials are well-known $LiCoO_2$ (with an energy density of about 518 Wh kg^{-1}), spinel $LiMn_2O_4$ (500 Wh kg^{-1}), and olivine $LiFePO_4$ (500 Wh kg^{-1}). But their energy densities are still somewhat too low to meet the requirements of practical EVs. Thus, researchers are struggling to search for new cathode materials with higher specific capacity, such as the lithium-rich mixed-metal oxides reported by Argonne [1,2]. Another strategy is to explore no-lithium metal oxides (e.g. MoO_3 [3], V_2O_5 [4]) and conducting polymers (e.g. polyaniline and polypyrrole [5]). Among these materials, vanadium oxide [6–10] and metal-vanadium-based oxides [11–14] have attracted much attentions recently. Poizot et al. reported a binary cathode system of Fe_2O_3—V_2O_5, which contains two components, i.e. $Fe_2V_4O_{13}$ and $FeVO_4$ [15]. The electrochemical performance of $FeVO_4{\cdot}nH_2O$ was also studied and it was found that the insertion capacity highly depends upon the water content [16–18]. However, little attention has been devoted to pure $Fe_2V_4O_{13}$ as a cathode material, which has the potential to deliver higher theoretical capacity than $FeVO_4$ in a wide voltage range because of the possible greater valence changes of V^{5+} and Fe^{3+} ions. In fact, $Fe_2V_4O_{13}$ can exhibit a high energy density of 738 Wh kg^{-1} according to this study, which is much higher than those of the polymeric cathodes as well as the conventional cathode materials.

Šurca et al. prepared crystalline $Fe_2V_4O_{13}$ films via a sol–gel method and investigated their electrochemical performance, but few details were given in their paper [19]. Recently, Patoux et al. introduced carbon black as a conductive additive in the crystalline $Fe_2V_4O_{13}$ electrode, which showed good cycling performance in the voltage range of 2.0–3.6 V [20]. Enhanced electrical conductivity during the lithiation and delithiation of the $Fe_2V_4O_{13}$ electrode was believed to be the key factor for the improvement.

Electrostatic spray deposition (ESD) technique is a facile method to fabricate carbon- and binder-free thin-film electrodes with porous structures [21]. A high porosity provides a sufficient space for a close contact between the electrolyte solution and the electrodes to reduce the impedance of the electrochemical cells using the porous electrodes. It has been successfully used to fabricate many nanostructured thin-film electrodes, particularly anode materials such as CoO—Li_2O and SnO_2—CuO—Li_2O composites [22–24], but few cathode films have been prepared [25]. In this paper, we apply the ESD technique to prepare $Fe_2V_4O_{13}$ films and investigate extensively their electrochemical performance. Special focus is paid to the effect of the crystallinity of a film on the electrochemical properties.

* Corresponding author. Tel.: +86 551 3606971; fax: +86 551 3601592.
E-mail address: cchchen@ustc.edu.cn (C.-H. Chen).

0925-8388/$ – see front matter © 2012 Elsevier B.V. All rights reserved.
doi:10.1016/j.jallcom.2011.12.092

2. Experimental

All the chemical reagents were analytical grade. Firstly, 2 mmol ammonia vanadate (NH_4VO_3), 1 mmol ferric nitrate ($Fe(NO_3)_3{\cdot}9H_2O$) and 2.5 mmol oxalic acid ($C_2H_2O_4{\cdot}H_2O$) were dissolved in a mixture of 5 mL H_2O and 5 mL ethanol at 70 °C. Then, 10 mL ethanol and 80 mL 1,2-propylene glycol were added into the solution which was subsequently cooled down to room temperature. The as-prepared light yellow solution was transferred to a syringe with a metal needle. Flat stainless steel discs with a diameter of 1.5 cm were used as the substrates and the distance between the needle and the substrate was about 2–3 cm. For each deposition, while a direct current (DC) voltage of 9–12 kV was applied between the substrate and the needle, the precursor solution in the syringe was fed to the needle at a constant flow rate of 1.0 mL min^{-1} by a syringe pump. A stable spray was thus generated towards the substrate which was heated at 290 °C. The deposition of each run lasted for 3 h. Thus thin films composed of iron and vanadium oxides were obtained. Then some of these films were annealed at 400 °C for 10 h in an electric furnace under ambient atmosphere. The amount of the active material in a thin film was about 1.0 mg and the area density of each electrode was about 0.65 mg cm^{-2}.

The morphology of the thin films was studied by scanning electron microscopy (SEM, JEOL-6390 LA). Their crystal structures were analyzed by X-ray diffraction (Philips X'Pert Pro Super, Cu Kα radiation). X-ray photoelectron spectroscopy (XPS) on the films was also performed at the XPS station in National Synchrotron Radiation Laboratory (VG Scienta-R3000, Al Kα sources). All the binding energies were calibrated to C 1s peak at 284.3 eV.

The electrochemical properties of the Fe/V-oxide thin films were characterized using CR2032 coin cells. Both of the as-deposited and annealed thin films were used as the working electrodes, and lithium metal was used as the counter electrode, while the electrolyte was 1.0 M $LiPF_6$ in ethylene carbonate/diethyl carbonate (1:1, v/v). The cells were assembled in an argon-filled glove box (MBRAUN LABMASTER 130) with moisture content and oxygen levels less than 1.0 ppm. The cells were cycled on a multi-channel battery cycler (NEWWARE BTS-610). Both cyclic voltammograms (CV) and AC impedance spectra of the cells were measured with an electrochemical work station (CHI 604b). For the CV measurement, the voltage ranges were set as 1.0–4.0 V and 2.5–4.0 V at a scan rate of 0.2 mV s^{-1}. For the impedance measurement, the frequency range used was 0.01–100 kHz with the AC amplitude of 5.0 mV.

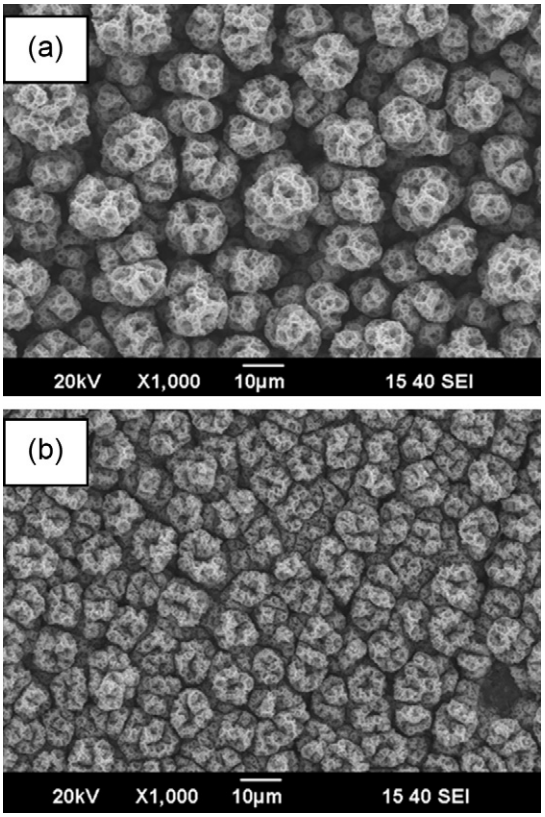

Fig. 1. SEM images of the Fe/V oxide thin films as deposited at 290 °C for 3 h (a) and annealed at 400 °C for 10 h (b).

3. Results and discussion

Fig. 1a shows the SEM image of the porous thin film deposited at 290 °C for 3 h. It is clear that the thin film is composed of rather porous spheres with a diameter of around 10 μm. The as-deposited thin films with ash-black color were further annealed in air in a furnace at 400 °C for 10 h to obtain orange-color thin films. After the annealing, the morphology of thin film can be largely retained except for some minor shrinkage, as shown in Fig. 1b. As electrodes, the films with a stable porous structure are beneficial for the capacity retention during the cycling [26,27]. On one hand, the porous structure can lead to a large contact area between the electrolyte and the electrode materials so that the diffusion length of lithium ions can be decreased significantly. On the other hand, the porous structure can alleviate the strain or stress in the electrodes due to the volume change during cycling [28,29]. Fig. 2 gives the XRD patterns of the thin films before and after the annealing at 400 °C, respectively. It can be seen that except for the peaks from the stainless steel substrate, no distinguished diffraction peaks are assigned to the as-deposited Fe/V-oxide thin film, which is therefore amorphous. After the annealing at 400 °C, the amorphous Fe/V-oxide thin film has crystallized and a series of diffraction peaks from 10° to 40°, which can be attributed to $Fe_2V_4O_{13}$ (JCPDF Card No. 89-5460), are observed.

Because V^{5+} ions may be reduced into V^{4+} in ethanol [30], and, during the ESD process of the Fe/V-oxide films, the precursor solution uses a mixed solvent system of ethanol and propylene glycol, lower oxidation states of V and Fe may be present in the thin films. Fig. 3 shows the XPS spectra of the V2p region and Fe2p region for the Fe/V-oxide thin films. For the amorphous thin film (Fig. 3a and b), both the peaks for $V2p_{3/2}$ and $Fe2p_{3/2}$ are detected. The binding energies of $V2p_{3/2}$ at 516.3 eV and 517.3 eV can be assigned to V^{4+} and V^{5+}, respectively [31,32]. Similarly, we can assign the binding energies of $Fe2p_{3/2}$ at 710.7 eV and 711.6 eV to Fe^{2+} and Fe^{3+}, respectively. The energy values measured here are consistent with the results of Mills et al. [33]. By means of curve fitting, the corresponding distribution of vanadium and iron species are estimated (Table 1). According to the quantitative results, it is suggested that the nominal composition of the amorphous thin film should be $Fe_2V_4O_{12.29}$. After the annealing at 400 °C in air, the V^{4+} and Fe^{2+} ions in the amorphous sample are oxidized into V^{5+} and Fe^{3+}, respectively (Fig. 3c and d), leading to the formation of a stoichiometric phase of $Fe_2V_4O_{13}$.

As mentioned above, there is no binder or conductive additive (such as carbon black) in these ESD-derived porous Fe/V-oxide thin films. Hence these films allow us to investigate the intrinsic

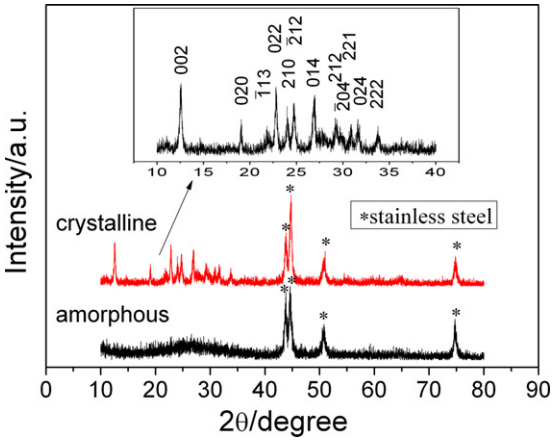

Fig. 2. XRD patterns of the as-deposited and annealed Fe/V oxide thin films.

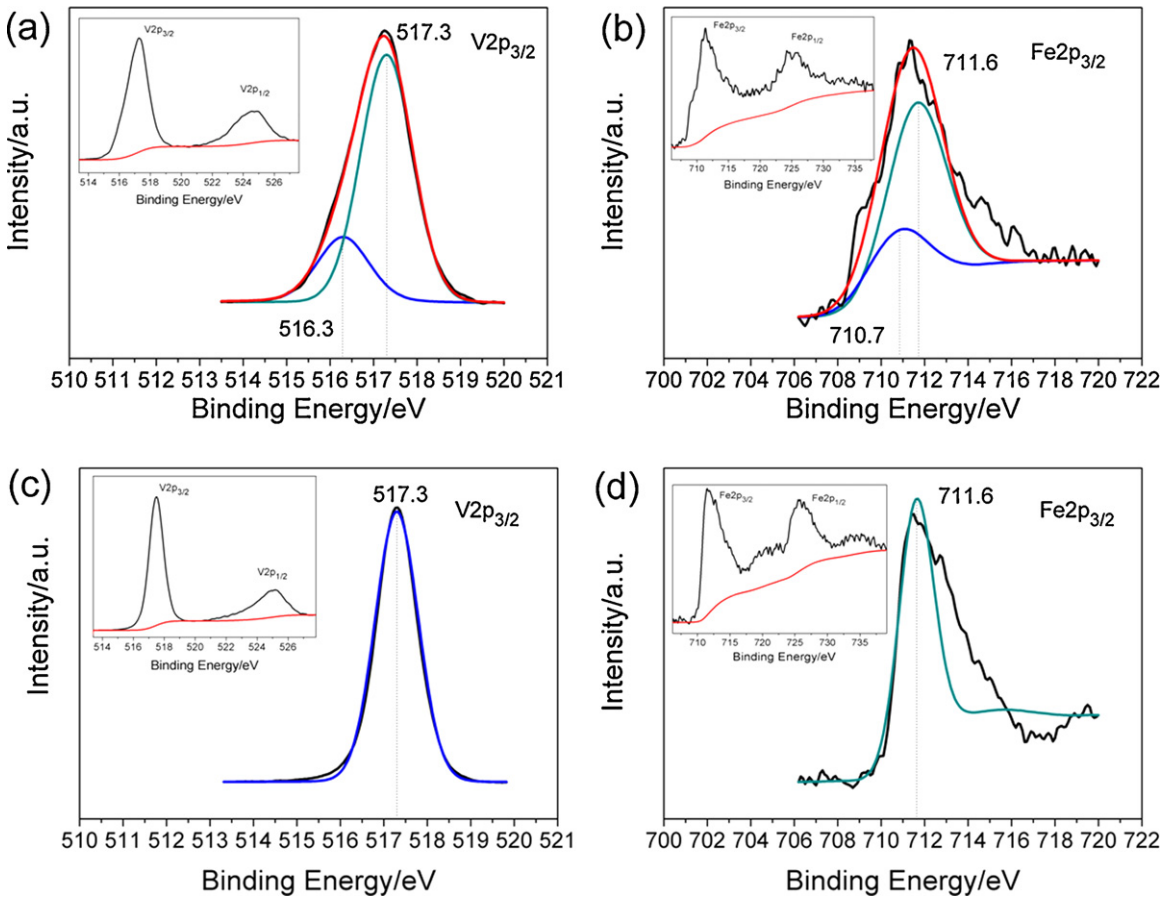

Fig. 3. XPS spectra of the Fe/V oxide thin films: V2p spectra (a) and Fe2p spectra (b) for amorphous thin film; V2p spectra (c) and Fe2p spectra (d) for crystalline thin film.

electrochemical performance of the complex Fe/V oxide thin films. Fig. 4 shows the cyclic voltammograms of two 400 °C-annealed Fe/V-oxide thin films and one as-deposited amorphous thin film at the scan rate of 0.2 mV s^{-1} with different lower cut-off voltages. Fig. 4a shows the first three cycles of a crystalline film in the voltage range of 1.0–4.0 V. During the initial lithiation, three peaks at 2.86, 2.36 and 1.71 V appear but disappear in the following cycles. This disappearance of the reduction peaks indicates that the $Fe_2V_4O_{13}$ film undergoes a structural degradation during the lithiation process. However, if the lower cut-off voltage is set at 2.5 V instead of 1.0 V, the redox peaks exhibit good reversibility (Fig. 4b). This means that the irreversible structural degradation of the $Fe_2V_4O_{13}$ film must occur at the potentials below 2.5 V vs. Li^+/Li. Furthermore, by carefully comparing Fig. 4a and b, the degradation should be associated with the reduction step at around 1.7 V. Nevertheless, as for the amorphous thin film with the cyclic voltammogram shown in Fig. 4c, no significant redox peaks are observed during the lithiation and delithiation processes in the voltage range of 1.0–4.0 V.

Table 1
Binding energy and percentage of total areas of $V2p_{3/2}$ and $Fe2p_{3/2}$ peaks for the amorphous Fe/V oxide thin film.

$V2p_{3/2}$			$Fe2p_{3/2}$		
E_b (eV)	Total area (%)	Assignment	E_b (eV)	Total area (%)	Assignment
517.3	77.8	V^{5+}	711.6	73	Fe^{3+}
516.3	22.2	V^{4+}	710.7	27	Fe^{2+}

Fig. 5 shows the electrochemical performance of the porous $Fe_2V_4O_y$ films, including the voltage profiles (Fig. 5a) and cycling performance (Fig. 5b) in the voltage range of 1.0–4.0 V. We have also measured the cycling performance of the thin films discharge/charge in the voltage range of 2.5–4.0 V (inset in Fig. 5b). For the crystalline $Fe_2V_4O_{13}$ thin film, it can deliver a specific capacity of 409 mAh g^{-1} in the first discharge step and the initial capacity loss is about 19.7%. Patoux et al. believe that iron in $Fe_2V_4O_{13}$ might be partly electrochemically active [20]. Šurca et al. conclude based on their ex situ IR spectroscopy on the $Fe_2V_4O_{13}$ electrode that during the discharge process V^{5+} and Fe^{3+} ions can be both reduced [19]. Hence both V^{5+} and Fe^{3+} in our $Fe_2V_4O_{13}$ samples are also believed to be electrochemically active in the voltage range of 1.0–4.0 V. For the amorphous $Fe_2V_4O_{12.29}$ film, it delivers a specific capacity of 349.9 mAh g^{-1} in the first discharge step and 244.9 mAh g^{-1} in the second discharge step with the initial capacity loss of 30%. Different from that of the amorphous $Fe_2V_4O_{12.29}$, the voltage profile of the crystalline $Fe_2V_4O_{13}$ shows some plateau-like features during the first discharge step, which disappears after the fist cycle, being corresponding well to the CV results (Fig. 4a). The XRD result (Fig. 6) indicates that the crystalline $Fe_2V_4O_{13}$ phase is degraded into amorphous after a discharge down to 1.0 V. All of the peaks can be attributed to the stainless steel and the plastic bag used to prevent the sample from oxidation in air. The cycling performances of the crystalline $Fe_2V_4O_{13}$ and amorphous $Fe_2V_4O_{12.29}$ films are shown in Fig. 5b. In the voltage range of 1.0–4.0 V, the amorphous $Fe_2V_4O_{12.29}$ film shows better capacity retention than the crystalline $Fe_2V_4O_{13}$ film. After 50 cycles, 80% of the second-cycle capacity can be retained for the

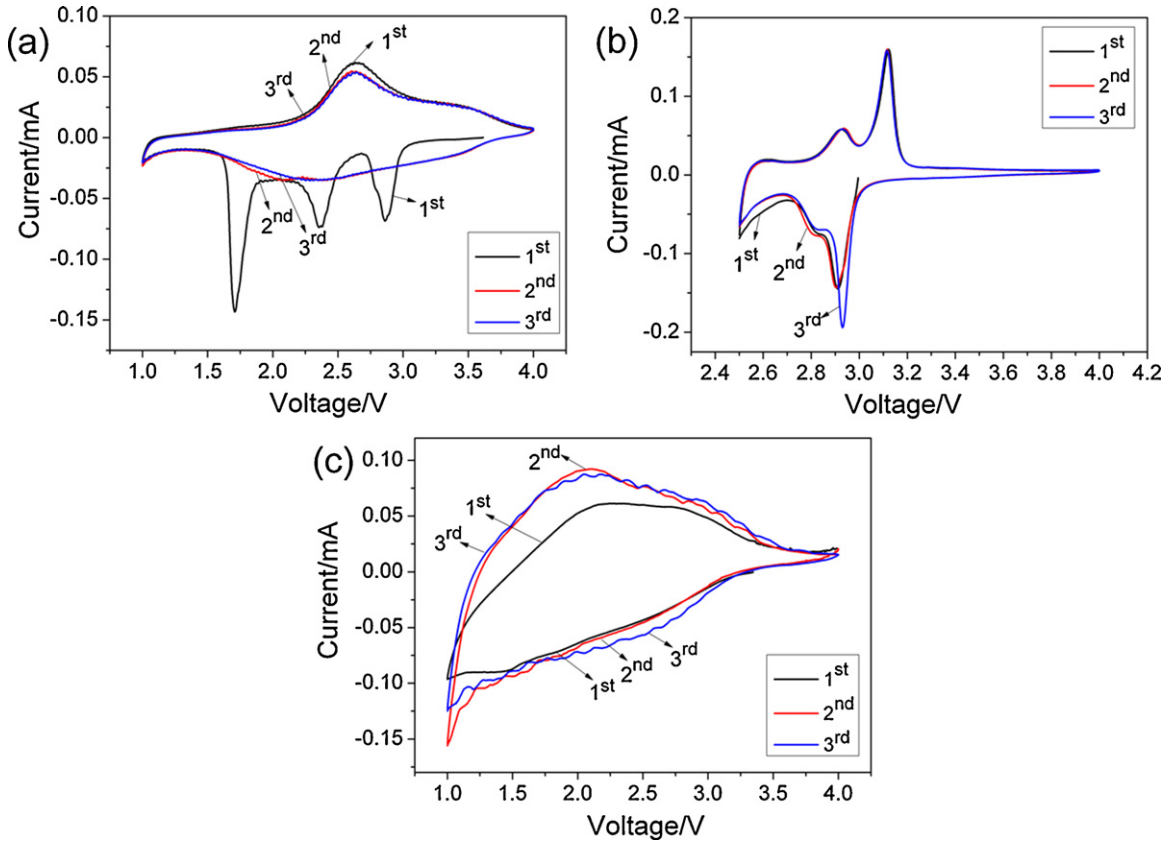

Fig. 4. Cyclic voltammograms of $Fe_2V_4O_y$/Li cells: crystalline film/Li (a and b) and amorphous film/Li (c). The scan rate was 0.2 mV s^{-1}.

amorphous film while only 65.2% is retained for the crystalline $Fe_2V_4O_{13}$ film. The better capacity retention of the amorphous film is partly attributed to the mixed valence states (e.g. V^{4+}/V^{5+} and Fe^{2+}/Fe^{3+}) in it as well as its much improved electronic conductivity during the cycling performance. Besides, the structural degradation of the crystalline electrode during the electrochemical cycling in a large voltage range (1.0–4.0 V here) is considered to be the main factor that explains its fast capacity fading. Similar phenomenon has also been found in silicon anode [34–36], MnO_2 cathode [37] and other vanadates electrodes such as $InVO_4$ [16].

In the voltage range of 2.5–4.0 V, a stable cycling performance of the crystalline film is obtained and a specific capacity of 70 mAh g^{-1} can be retained after 50 cycles. Such a good cycling performance can be ascribed to the stable structure during the charge and discharge processes in this relatively narrow voltage range. This is consistent with the CV results (Fig. 4b). However, for the amorphous film, a quite low reversible capacity of only 10 mAh g^{-1} is measured and a much greater initial capacity loss of 50% occurs (compared with only 8% for the crystalline film). In addition, in comparison with that of the amorphous film, the better cycleability of the crystalline sample suggests that the structure of $Fe_2V_4O_{13}$ in the voltage range of 2.5–4.0 V is stable.

For the purpose of applications of LIBs in EVs or HEVs, the electrode materials with a good rate capability are required. The rate capability test has been conducted on these two thin films. Due to the higher electronic conductivity resulted from the existences of small amount of V^{4+} and Fe^{2+} ions, the amorphous $Fe_2V_4O_{12.29}$ film exhibits better rate capability than crystalline $Fe_2V_4O_{13}$ (Fig. 7). At the current density of 0.88 mA cm^{-2}, the specific capacity of the amorphous $Fe_2V_4O_{12.29}$ film is almost one time higher than that of the crystalline $Fe_2V_4O_{13}$ film. This result makes it possible for the amorphous thin film to be a very attractive electrode material to develop high power LIBs.

Fig. 8 compares the AC impedance spectra of the half-cells made of the crystalline and the amorphous $Fe_2V_4O_y$ thin films. It is noticed that, compared with the crystalline $Fe_2V_4O_{13}$ film, the amorphous $Fe_2V_4O_{12.29}$ film exhibits much lower impedance. This result confirms again the amorphous film would give rise to lower impedance and better rate capability.

The ex situ SEM image of the crystalline thin film after 50 cycles in the voltage range of 1.0–4.0 V is shown in Fig. 9. It can be clearly seen that the morphology of the thin film can be mostly retained after the electrochemical cycling. This suggests that the structural change from crystalline to amorphous (Fig. 6) does not influence substantially the film morphology. We expect that the morphology of the amorphous film should be even more stable because no crystalline structure is involved during the cycling.

It should be pointed out that this complex oxide cannot be used in the similar situation as for a traditional cathode material such as $LiCoO_2$ because there is no active lithium in its initial composition. To be used as a potential cathode, it must be coupled to a negative electrode material with active lithium (e.g. metallic lithium or lithiated graphite). It can provide much higher specific capacity when compared to some new-type cathode materials such as conductive polymers [5]. Also, it is advantageous for the amorphous $Fe_2V_4O_{12.29}$ when compared with V_2O_5 alone because V_2O_5 usually shows poor cycling performance and poor rate capability in an even narrower voltage range of 1.5–3.75 V [38]. Thus, we believe the current study represents a progress in Fe—V—O electrodes.

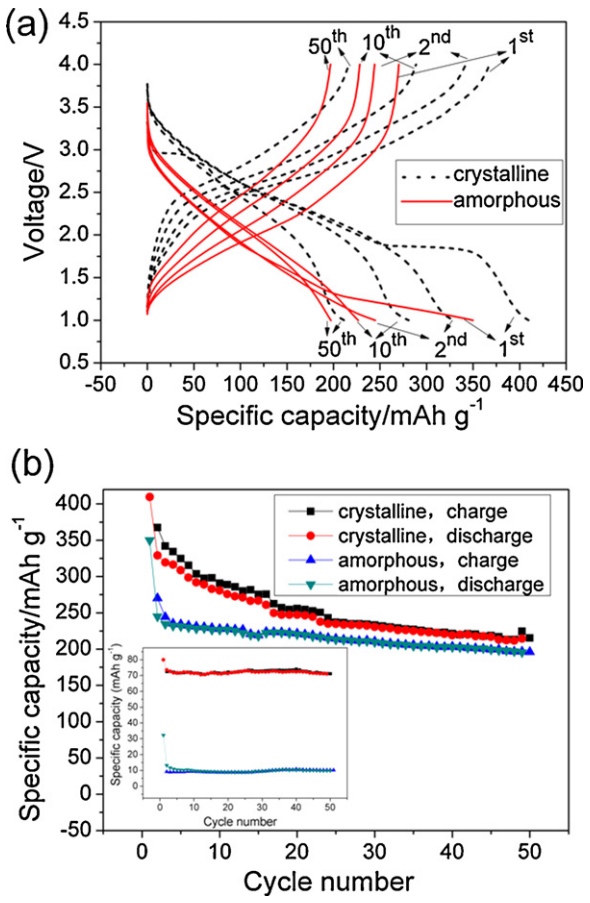

Fig. 5. The electrochemical performance of Fe/V-oxide thin-film electrodes: voltage profile (a), cycling performance in 1.0–4.0 V (b) and in 2.5–4.0 V (insert b) at a low current density (0.025 mA cm^{-2} for crystalline $Fe_2V_4O_{13}$ and 0.044 mA cm^{-2} for amorphous $Fe_2V_4O_{12.29}$).

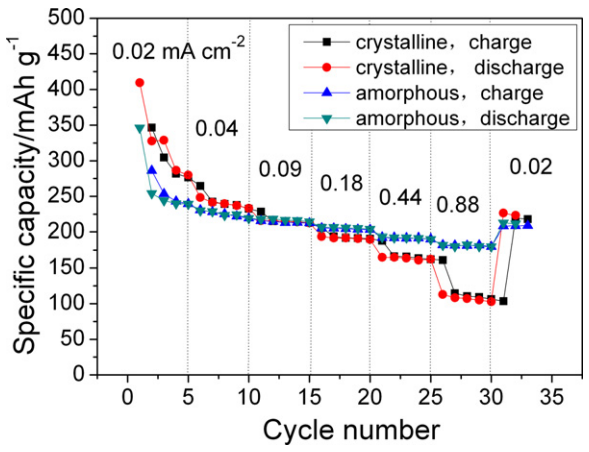

Fig. 7. Rate capability of Fe/V-oxide thin-film electrodes. The charge rate was all 0.02 mA cm^{-2}.

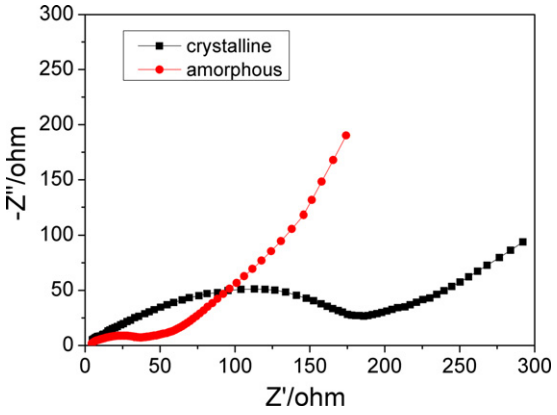

Fig. 8. AC impedance spectra of $Fe_2V_4O_y$/Li cells after being charged to 2.65 V at the 5th cycle.

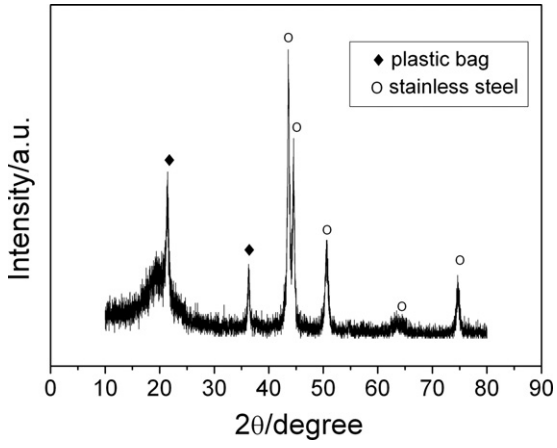

Fig. 6. Ex situ XRD pattern of the crystalline $Fe_2V_4O_{13}$ thin-film electrode after being discharged to 1.0 V vs. Li^+/Li.

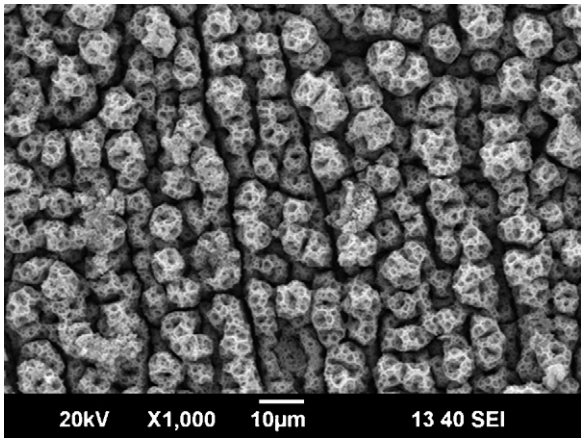

Fig. 9. Ex situ SEM image of the crystalline $Fe_2V_4O_{13}$ thin film after 50 cycles.

4. Conclusions

Porous amorphous $Fe_2V_4O_{12.29}$ and crystalline $Fe_2V_4O_{13}$ thin films have been prepared by the electrostatic spray deposition technique. Structural degradation occurs for the crystalline $Fe_2V_4O_{13}$ thin film in the voltage range of 1.0–4.0 V while the amorphous $Fe_2V_4O_{12.29}$ thin film shows good cycling performance and rate capability due to the enhanced electronic conductivity caused by the existence of mixed valence states of Fe and V. This new vanadium-based oxide can be a promising electrode material for high power lithium batteries.

Acknowledgments

This study was supported by National Science Foundation of China (Grant Nos. 20971117 and 10979049) and Education Department of Anhui Province (Grant No. KJ2009A142). We are also grateful to the Solar Energy Operation Plan of Academia Sinica.

References

[1] M.M. Thackeray, S.H. Kang, C.S. Johnson, J.T. Vaughey, R. Benedek, S.A. Hackney, J. Mater. Chem. 17 (2007) 3112.
[2] S.H. Kang, M.M. Thackeray, Electrochem. Commun. 11 (2009) 748.
[3] L. Zhou, L.C. Yang, P. Yuan, J. Zou, Y.P. Wu, C.Z. Yu, J. Phys. Chem. C 114 (2010) 21868.
[4] S.Q. Wang, S.R. Li, Y. Sun, X.Y. Feng, C.H. Chen, Energy Environ. Sci. 4 (2011) 2854.
[5] Y.H. Huang, J.B. Goodenough, Chem. Mater. 20 (2008) 7237.
[6] A. Sakunthala, M.V. Reddy, S. Selvasekarapandian, B.V.R. Chowdari, P.C. Selvin, Energy Environ. Sci. 4 (2011) 1712.
[7] Y.L. Cheah, N. Gupta, S.S. Pramana, V. Aravindan, G. Wee, M. Srinivasan, J. Power Sources 196 (2011) 6465.
[8] X.H. Rui, J.X. Zhu, W.L. Liu, H.T. Tan, D.H. Sim, C. Xu, H. Zhang, J. Ma, H.H. Hng, T.M. Lim, Q.Y. Yan, RSC Adv. 1 (2011) 117.
[9] D.M. Yu, S.T. Zhang, D.W. Liu, X.Y. Zhou, S.H. Xie, Q.F. Zhang, Y.Y. Liu, G.Z. Cao, J. Mater. Chem. 20 (2010) 10841.
[10] A.Q. Pan, J.G. Zhang, Z.M. Nie, G.Z. Cao, B.W. Arey, G.S. Li, S.Q. Liang, J. Liu, J. Mater. Chem. 20 (2010) 9193.
[11] W.D. Huang, S.K. Gao, X.K. Ding, L.L. Jiang, M.D. Wei, J. Alloys Compd. 495 (2010) 185.
[12] C.A. Cai, D.S. Guan, Y. Wang, J. Alloys Compd. 509 (2011) 909.
[13] S.B. Ni, D.Y. He, X.L. Yang, T. Li, J. Alloys Compd. 509 (2011) L142.
[14] Z.Y. Huang, H.M. Zeng, L. Xue, X.G. Zhou, Y. Zhao, Q.Y. Lai, J. Alloys Compd. 509 (2011) 10080.
[15] P. Poizot, S. Laruelle, M. Touboul, J.-M. Tarascon, C.R. Chim. 6 (2003) 125.
[16] S. Denis, E. Baudrin, F. Orsini, G. Ouvrard, M. Touboul, J.-M. Tarascon, J. Power Sources 81–82 (1999) 79.
[17] S. Denis, R. Dedryve're, E. Baudrin, S. Laruelle, M. Touboul, J. Olivier-Fourcade, J.C. Jumas, J.-M. Tarascon, Chem. Mater. 12 (2000) 3733.
[18] P. Poizot, E. Baudrin, S. Laruelle, L. Dupont, M. Touboul, J.-M. Tarascon, Solid State Ionics 138 (2000) 31.
[19] A. Šurca, B. Orel, U.O. Krašovec, U.L. Štangar, G. Dražič, J. Electrochem. Soc. 147 (2000) 2358.
[20] S. Patoux, T.J. Richardson, Electrochem. Commun. 9 (2007) 485.
[21] C.H. Chen, E.M. Kelder, P.J.J.M. van der Put, J. Schoonman, J. Mater. Chem. 6 (1996) 765.
[22] Y. Yu, C.H. Chen, J.L. Shui, S. Xie, Angew. Chem. Int. Ed. 44 (2005) 7085.
[23] Y. Yu, C.H. Chen, Y. Shi, Adv. Mater. 19 (2007) 993.
[24] Y. Yu, Y. Shi, C.H. Chen, Nanotechnology 18 (2007) 055706.
[25] L. Wang, L.C. Zhang, I. Lieberwirth, H.W. Xu, C.H. Chen, Electrochem. Commun. 12 (2010) 52.
[26] C.K. Chan, H. Peng, R.D. Twesten, K. Jarausch, X.F. Zhang, Y. Cui, Nano Lett. 7 (2007) 490.
[27] C. O'Dwyer, V. Lavayen, D.A. Tanner, S.B. Newcomb, E. Benavente, G. González, C.M.S. Torres, Adv. Funct. Mater. 19 (2009) 1736.
[28] L.J. Fu, T. Zhang, Q. Cao, H.P. Zhang, Y.P. Wu, Electrochem. Commun. 9 (2007) 2140.
[29] Q.T. Qu, L.J. Fu, X.Y. Zhan, D. Samuelis, J. Maier, L. Li, S. Tian, Z.H. Li, Y.P. Wu, Energy Environ. Sci. 4 (2011) 3985.
[30] N. Ding, S.H. Liu, C.H. Chen, I. Lieberwirth, Appl. Phys. Lett. 93 (2008) 173510.
[31] R.J. Colton, A.M. Guzman, J.W.J. Rabalais, Appl. Phys. 49 (1978) 409.
[32] J.L.G. Fierro, L.A. Arrua, J.M.L. Nieto, G. Kremenic, Appl. Catal. 37 (1988) 323.
[33] P. Mills, J.L. Sullivan, J. Phys. D 16 (1983) 723.
[34] T. Takamura, S. Ohara, M. Uehara, J. Suzuki, K. Sekine, J. Power Sources 129 (2004) 96.
[35] T.D. Hatchard, J.R. Dahn, J. Electrochem. Soc. 151 (2004) A838.
[36] J. Li, J.R. Dahn, J. Electrochem. Soc. 154 (2007) A156.
[37] Q.T. Qu, P. Zhang, B. Wang, Y.H. Chen, S. Tian, Y.P. Wu, R. Holze, J. Phys. Chem. C 113 (2009) 14020.
[38] S.L. Chou, J.Z. Wang, J.Z. Sun, D. Wexler, M. Forsyth, H.K. Liu, D.R. MacFarlane, S.X. Dou, Chem. Mater. 20 (2008) 7044.